Comparison of murine and human estrogen sulfotransferase inhibition in vitro and in silico–implications for differences in activity, subunit dimerization and substrate inhibition

Eva Stjernschantz, Jelle Reinen, Walter Meinl, Beena J. George, Hansruedi Glatt, Nico P.E. Vermeulen, Chris Oostenbrink

Accepted Manuscript

Title: Comparison of murine and human estrogen sulfotransferase inhibition in vitro and in silico–implications for differences in activity, subunit dimerization and substrate inhibition

Authors: Eva Stjernschantz, Jelle Reinen, Walter Meinl, Beena J. George, Hansruedi Glatt, Nico P.E. Vermeulen, Chris Oostenbrink

PII: S0303-7207(09)00583-8
DOI: doi:10.1016/j.mce.2009.12.001
Reference: MCE 7382

To appear in: *Molecular and Cellular Endocrinology*

Received date: 22-9-2009
Revised date: 31-10-2009
Accepted date: 2-12-2009

Please cite this article as: Stjernschantz, E., Reinen, J., Meinl, W., George, B.J., Glatt, H., Vermeulen, N.P.E., Oostenbrink, C., Comparison of murine and human estrogen sulfotransferase inhibition in vitro and in silico–implications for differences in activity, subunit dimerization and substrate inhibition, *Molecular and Cellular Endocrinology* (2008), doi:10.1016/j.mce.2009.12.001

Comparison of murine and human estrogen sulfotransferase inhibition *in vitro* and *in silico* – implications for differences in activity, subunit dimerization and substrate inhibition

Eva Stjernschantz*, [1], Jelle Reinen*, [1], Walter Meinl[2], Beena J. George[1], Hansruedi Glatt[2], Nico P.E. Vermeulen[1], Chris Oostenbrink[1,@]

*Both authors contributed equally

[1]Leiden/Amsterdam Centre for Drug Research - Division of Molecular Toxicology, Department of Chemistry and Pharmaceutical Sciences, Vrije Universiteit, De Boelelaan 1083, 1081 HV Amsterdam, The Netherlands. [2]Deutsches Institut für Ernährungsforschung, Potsdam-Rehbrücke, Germany.

[@]To whom correspondence should be addressed: c.oostenbrink@few.vu.nl

Phone: +31 20 5987606, Fax: +31 20 5987610

Keywords

estrogen sulfotransferase; substrate inhibition; molecular dynamics; simulation

Abbreviations

ED, endocrine disruption; EDC, endocrine disrupting compound; SULT1E1, sulfotransferase 1E1 (with prefix h and m for human and murine form, respectively); E2, 17β-estradiol; ER, estrogen receptor; PAPS, 3'-phosphoadenosine 5'-phosphosulfate; E1, estrone; PAP, 3'-phosphoadenosine 5'-phosphate; OHP, 1-hydroxypyrene; DES, diethylstilbestrol; DIS, dienestrol; αE2, 17α-estradiol; EE2, 17α-ethinylestradiol; E3, estriol; DHEA, dehydroepiandrosterone; RMS, root-mean-square; MD, molecular dynamics

Abstract

It is well established that various endocrine disrupting compounds (EDCs) can inhibit human estrogen sulfotransferase (SULT1E1). In this study, we investigate murine SULT1E1 inhibition *in vitro* and *in silico* and compare this to data for the human enzyme. 34 potential EDCs were screened for their ability to inhibit both murine and human SULT1E1 and IC_{50} values were determined for 14 of the inhibitory EDCs. Only estrone, dienestrol and enterolactone showed significant differences in affinity between the human and murine SULT1E1. Extensive molecular modelling was performed using molecular dynamics (MD) simulations. During the MD simulations the ligands moved away from the catalytically active position, something which was not observed when simulating the unit cell of the crystal structure. This finding suggests that catalytically inactive binding modes, other than the one observed in the crystal structures, are possible in SULT1E1. The ligands stayed longer in the catalytically active position in mSULT1E1, which is likely a result of simultaneous hydrogen bond formation on both sides of the binding pocket, which does not seem to be possible in hSULT1E1. The ligands in the human protein moved to a sub-pocket near the entrance of the active site, which offers hydrogen bond formation possibilities with Asp22 and Lys85 as well as favourable hydrophobic interactions. The ligands moved more randomly in mSULT1E1. These observations offer a possible explanation for the substrate inhibition only observed in hSULT1E1.

1 Introduction

The presence of estrogens in the environment and their possible role in the process of endocrine disruption (ED) has been the subject of a large number of studies in the past years (Bolger 1998; Harris 2004; Hotchkiss 2008). Endocrine disrupting compounds (EDCs) can interfere with the endocrine system by either mimicking or preventing the action of physiological hormones. They can also act by altering the synthesis and function of hormone receptors and by modifying the synthesis, transport, metabolism and excretion of hormones (Ropero 2006).

Estrogen sulfotransferase (SULT1E1) is an important enzyme involved in the metabolism of 17β-estradiol (E2), the natural ligand of the mammalian estrogen receptors (ERs). This cytosolic sulfotransferase catalyzes the transfer of a sulfuryl group (SO_3^-) from the ubiquitous donor 3'-phosphoadenosine 5'-phosphosulfate (PAPS) to E2 and other estrogens at the 3-hydroxy position. The resulting estrogen sulfates are highly water-soluble and unable to bind to the ER; instead they are either excreted from the cell or stored for reactivation by sulfatases (Strott 1996; Song 2000; Negishi 2001). SULT1E1 shows high affinity for E2 and estrone (E1) and is involved in the regulation of E2 responsiveness at physiological concentrations (Zhang 1998; Glatt 2004). It is believed that SULT1E1 plays an important role in protecting peripheral tissues from excessive estrogenic effects. Increased local availability of biologically active estrogens caused by decreased SULT1E1 expression or SULT1E1 inhibition may be related to various estrogen-dependent properties, such as the development and maintenance of hormone-dependent breast carcinomas (Qian 1998; Suzuki 2003; Utsunomiya 2004). Due to the critical role in controlling local estrogen levels, it is

important to understand the mechanism of SULT1E1, as well as to identify EDCs that inhibit this enzyme.

The function and reaction mechanism of cytosolic sulfotransferases have been studied extensively through structural as well as mutational and kinetic studies (Kakuta 1997; Kakuta 1998b; Zhang 1998; Pedersen 2002; Hoff 2006; Tyapochkin 2008). The reaction mechanism has been proposed to be of a sequential kinetic nature, involving the formation of a ternary enzyme complex before the products are released. This sequential mechanism can either proceed in an ordered bi-bi fashion, where the cofactor and the substrate bind in an ordered sequence, or through a random bi-bi mechanism, as displayed in Figure 1. Both random and ordered sequential mechanisms can lead to dead-end complexes and both mechanisms have been proposed for cytosolic sulfotransferases (Zhang 1998; Chapman 2004; Gamage 2005; Hoff 2006; Allali-Hassani 2007).

The sulfuryl transfer reaction has been proposed to proceed through an inline, S_N2-like displacement mechanism, involving a nucleophilic attack on the cofactor sulfonate by the substrate (Kakuta 1998b). A highly conserved histidine residue (His107 in hSULT1E1) is believed to deprotonate the hydroxyl group of the substrate, which can subsequently attack the sulfur atom of the cofactor, as displayed in Figure 2. In addition to His107, studies indicate two other residues important for catalysis (Kakuta 1997; Kakuta 1998b). Lys105 positions the substrate close to the cofactor and interacts with the sulfonate, thereby stabilizing the transition state. Lys47 seems to stabilize the transition state through donating a proton to the bridging oxygen of the cofactor, acting as a catalytic acid, and interacts with one of the sulfonate oxygens. His107 also seems to serve a stabilizing role through interaction with another of the sulfonate oxygens (Kakuta 1997; Kakuta 1998b). Until recently all crystal

structures contained either active cofactor, PAPS, and no substrate, or inactive cofactor, PAP, co-crystallized with different substrates. Earlier this year, Teramoto *et al* published a crystal structure of mouse sulfotransferase SULT1D1 in complex with both PAPS and substrate. This structure confirms the results of the previous studies (Teramoto 2009).

Several studies have shown that hSULT1E1 and other members of the sulfotransferase family exhibit substrate inhibition at higher substrate concentrations, as well as non-competitive binding of inhibitors (Falany 1995; Kester 2000; Kester 2002; Tyapochkin 2008). Other reports suggest non-productive substrate binding modes or binding of multiple substrates in the active site of different sulfotransferases (Rehse 2002; Gamage 2003; Lee 2003; Barnett 2004). There has been considerable debate in the literature whether these observations originate from the presence of a second, allosteric, binding site or can be explained by the formation of a dead-end complex through the binding of substrates or inhibitors to the enzyme with bound inactive cofactor, PAP (Zhang 1998; Cui 2004; Gamage 2005). No allosteric site outside the active site has been identified in any of the published crystal structures. However, most of the substrate-containing structures result from crystal soaking experiments, which may prevent the binding of the substrate to an external allosteric site, if large conformational changes are required (Shevtsov 2003). Zhang *et al* suggested that in the dimeric hSULT1E1, one of the active sites is the catalytic site, whereas the other serves as an allosteric site, regulating catalysis through substrate inhibition (Zhang 1998). Gamage *et al* proposed that a second molecule in the active site could be the reason for substrate inhibition of human SULT1A1 at high substrate concentrations (Gamage 2003). Alternatively, substrate binding in a non-productive binding mode in the active site at high concentrations could be the origin of substrate inhibition (Gamage 2005).

Unlike most sulfotransferases, mSULT1E1 does not seem to display substrate inhibition to the same extent as the human enzyme (Falany 1997; Kakuta 1998a; Qian 1999). The crystal structures of human and murine SULT1E1 bound to their natural substrate E2 have been published and show high similarity both in structure and mode of substrate binding (Pedersen 2002). A significant difference between the murine and human enzyme is that the murine enzyme is biologically active as a monomer, whereas the human one only functions as a dimer (Petrotchenko 2001). It is therefore interesting to study whether the apparent differences between the human and murine SULT1E1, in terms of substrate inhibition and differences in biologically active forms of the proteins, correlate with a functional difference between human and murine SULT1E1 and what the origin of this possible functional difference is.

We have recently developed a fluorescence HPLC-based screening assay for inhibition of hSULT1E1 (Reinen 2006) which makes use of the nonradioactive and non-carcinogenic substrate 1-hydroxypyrene (OHP) and hSULT1E1 expressed in *Salmonella typhimurium*. Here we compare the enzymatic and inhibitory properties of human and murine SULT1E1 *in vitro* and *in silico*. The aim was to investigate whether this comparison can elucidate the basis for substrate inhibition and the possible reasons for the existence of different biologically active forms of sulfotransferases in different organisms. Extensive molecular modeling was used to rationalize the experimental findings and to suggest possible explanations to the contradictory findings presented in literature.

2 Materials and methods

2.1. Chemicals

Ethylenediaminetetraacetic acid (EDTA) and dithiothreitol (DTT) were obtained from Applichem (Lokeren, Belgium). Aldrin, endrin, enterolactone, endosulfan sulfate, vinclozolin, hexachlorobenzene (HCB), potassium dihydrogenphosphate (KH_2PO_4), dipotassium hydrogenphosphate (K_2HPO_4), ammonium acetate (NH_4CH_3COOH), acetic acid (AcOH), ethanol (EtOH) and dimethyl sulfoxide (DMSO) were obtained from Riedel de Haën (Seelze, Germany). Acros (Geel, Belgium) supplied nonylphenol. HPLC-grade acetonitrile (ACN), 3'-phosphoadenosine-5'-phosphosulfate (PAPS), 1-hydroxypyrene (OHP), all inhibitors and all other chemicals were purchased from Sigma-Aldrich (Zwijndrecht, The Netherlands).

The syntheses of (±)-4-(α-hydroxyethyl)pyrene (1-HEP), 6-hydroxymethyl-benzo[*a*]pyrene (6-HMBP), 11-hydroxymethylbenzo[*a*]pyrene (11-HMBP), (±)-6-(α-hydroxyethyl)benzo[*a*]pyrene (6-HEBP) and 10-hydroxycyclopenta[*mno*]benzo[*a*]pyrene (10-HCPBP) will be described elsewhere (C. Donath *et al.*, to be published). All these benzylic alcohols were bioactivated to mutagens by hSULTs and mSULTs (C. Donath *et al.*, to be published) and therefore are expected to compete with the conjugation of other substrates by these enzymes.

2.2 Cytosolic preparations

The cDNA of mouse SULT1E1 (mSULT1E1; GenBank accession no. NM 023135) was cloned and expressed in *Escherichia coli* XL-1 Blue cells using the pKK233-2 expression

vector as previously described for the various human sulfotransferases (Falany 1995). The plasmid was adapted to the restriction enzymes of *Salmonella typhimurium* LT2 by passing it through the restriction-deficient, but methylation-proficient *Salmonella typhimurium* strain LB5000. The plasmid was then used to transform the *his*$^-$ strain TA1538. The newly generated *Salmonella typhimurium* strain was designated TA1538-mSULT1E1. mSULT1E1 constituted approximately 5% of the total cytosolic protein.

The transformed bacterial strain was grown overnight in the presence of ampicillin (100 μg/ml) to reinforce the maintenance of the recombinant plasmid. Bacterial cytosol was prepared by ultrasonication and dialyzed for 4 h against a 100-fold excess of buffer (150 mM KCl in 10 mM sodium phosphate buffer (pH 7.4)) (Glatt 1995a; Glatt 1995b).

Human SULT1E1 (hSULT1E1) and SULT1A1 (hSULT1A1) were expressed as described previously (Reinen 2006). Bacterial cytosol was prepared as described above. The use of *Salmonella* cytosol has advantages over the use of purified SULTs. Stabilization was observed for various SULTs (e.g. SULT1A1) in the presence of the cytosolic proteins. Moreover, *Salmonella* cytosol rapidly degrades PAP (H. R. Glatt, unpublished result), the product formed from PAPS during the sulfuryl transfer reaction, which is a potent inhibitor of various SULTs, including human SULT1A1 (Rens-Domiano 1987) and hSULT1E1 (Zhang 1998).

2.3. HPLC analysis of 1-hydroxypyrene and pyrene 1-sulfate

In order to measure the sulfonation of 1-hydroxypyrene, HPLC analysis was performed as reported previously (Reinen 2006). Extracts (50 μl) from cytosolic fractions of

mSULT1E1 incubated with OHP were analyzed for the formation of pyrene 1-sulfate by HPLC (pumps 303 and 305, manometer 805, dynamic mixer 811B and auto-injector 234, manufactured by Gilson, Middleton, USA) using a reversed phase C-18 column (ChromSpher 5 µm, 100 mm x 3 mm, Chrompack, The Netherlands) and a gradient elution with solvent A (5% ACN 10 mM ammonium acetate (pH 5)) and solvent B (90% ACN 10 mM ammonium acetate (pH 5)). A linear gradient from 5 to 90% ACN in 4.5 min, constant for 4 min, and back to 5% ACN in 0.5 min followed by 6 min equilibration at 5% was applied. The flow rate of the mobile phase was 0.5 ml/min. Detection was accomplished with a fluorescence spectrophotometer (λ_{ex} = 346 nm, λ_{em} = 384 nm; RF-10A$_{XL}$, Shimadzu, Kyoto, Japan). Peak areas of OHP and pyrene 1-sulfate were quantified by the Shimadzu Class VP 4.3 software package.

Since no chemically prepared pyrene 1-sulfate was available, calibration curves of pyrene 1-sulfate were made as described previously (Reinen 2006). Briefly, OHP was incubated in the presence of PAPS and hSULT1A1 with a resulting pyrene 1-sulfate yield of more than 97% in all cases (Ma 2003). These calibration curves were made for each single enzyme kinetic experiment to accurately determine the amounts of pyrene 1-sulfate formed using the HPLC analysis procedure described above.

2.4. Protein and time dependency and enzyme kinetics of murine SULT1E1-mediated pyrene 1-sulfate formation

Linearity of the protein-dependent formation of pyrene 1-sulfate and its time dependency were investigated preceding the inhibition studies. Protein dependency was investigated by incubating 200 µl of a mixture containing 250 nM OHP, 12.5 µM PAPS and

different mSULT1E1 concentrations (6.25 – 93.75 ng/ml) in a 100 mM phosphate buffer (pH 7.4) containing 2 mM EDTA and 1 mM DTT. The mixtures were incubated at 37 °C for 30 min. The incubations were terminated by addition of 200 µl ice-cold ACN. Sample preparation was performed as described above and the amount of pyrene 1-sulfate formed was determined using HPLC analysis (see above).

Linearity of the formation of pyrene 1-sulfate in time was investigated by incubating 200 µl of a mixture containing 18.75 nM OHP, 25 ng/ml mSULT1E1 (equivalent to 0.5 µg/ml of total protein of the cytosolic fraction), and 12.5 µM PAPS at 37 °C in a 100 mM phosphate buffer (pH 7.4) containing 2 mM EDTA and 1 mM DTT. Incubations were stopped at different time-points by addition of 200 µl ice-cold ACN.

Enzyme kinetics were determined by adding 50 µl of 50 µM PAPS to 150 µl of a mixture containing 5 ng mSULT1E1 and OHP concentrations ranging from 0 to 750 nM (9 concentrations) in a 100 mM phosphate buffer (pH 7.4) containing 2 mM EDTA and 1 mM DTT. The mixtures were incubated at 37 °C for 30 min. The incubations were terminated by addition of 200 µl ice-cold ACN. Sample preparation was performed as described above and the amount of pyrene 1-sulfate formed was determined using HPLC analysis (see above).

Reaction rates were calculated and plotted against the substrate concentrations to obtain Michaelis-Menten curves, and the 'one site binding hyperbola' fitting module of GraphPad Prism 3.0 was used to estimate K_m and V_{max} values.

2.5. SULT1E1 inhibition screening

After optimizing the mSULT1E1 assay conditions, the ability of the assay to identify mSULT1E1 inhibitors was tested with a selection of 34 known EDCs. This selection included 19 EDCs which were used previously for hSULT1E1 inhibition screening under almost identical conditions (Reinen 2006). The reactions were initiated by adding 50 µl of 50 µM PAPS to 150 µl of a mixture containing 10 ng mSULT1E1, 250 nM OHP, and 2.5 µM of each library compound in a 100 mM phosphate buffer (pH 7.4) containing 2 mM EDTA and 1 mM DTT. The mixtures were incubated at 37 °C for 30 min and reactions were terminated by adding 200 µl ice-cold ACN. Sample preparation and determination of the amount of formed pyrene 1-sulfate by HPLC was performed as described above.

The 15 compounds in the EDC selection which had not been investigated for inhibition of the orthologous human enzyme, hSULT1E1, before were tested at the same concentration (2.5 µM) using the hSULT1E1 inhibition screening assay described previously (Reinen 2006).

2.6. IC_{50} measurements

The IC_{50} values were determined for a selection of 14 EDCs. These included the 10 EDCs for which IC_{50} values had previously been determined for hSULT1E1 (Reinen 2006) and four additional EDCs (testosterone, progesterone, resveratrol and enterolactone). In a total volume of 200 µl, 250 nM OHP, 50 ng/ml mSULT1E1, and 12.5 µM PAPS were incubated at 37 °C for 30 min in the presence and absence of various concentrations of the SULT1E1 inhibiting compounds. The incubations were terminated by addition of 200 µl ice-cold acetonitrile. Sample preparation and determination of the amount of formed pyrene-1-sulfate by HPLC was performed as described above. IC_{50} measurements were also performed to

investigate the inhibition of hSULT1E1 by testosterone, progesterone, resveratrol and enterolactone as described previously (Reinen 2006).

2.7. Computer modelling

The sequences of murine and human SULT1E1, PDB codes 1AQU (Kakuta 1997) and an E2- and PAP-bound hSULT1E1, were aligned and the structures superposed and compared, using Molecular Operating Environment (MOE). 1AQU is the murine structure co-crystallized with E2 and inactive cofactor PAP. Missing residues forming the loop Asp66 - Glu72 were modeled in using MOE. This loop is at the surface of the protein and far away from the active site. For comparison, automated docking calculations were performed for E2 and other ligands from this study to the substrate-free hSULT1E1 structure, using GOLD (Jones 1997). The hSULT1E1 structure in complex with PAP and E2 (Pedersen 2002) was kindly made available to us by Negishi *et al*. This structure is very similar to the PAPS-bound apo-structure of hSULT1E1, PDB code 1HY3 (Pedersen 2002).

To further study the differences between the SULT1E1 structures, molecular dynamics simulations were performed on the resulting docked complexes using the GROMOS05 (Christen 2005) and GROMACS (Berendsen 1995; Lindahl 2001) biomolecular simulation packages and the GROMOS force field parameter set 45A4 (Schuler 2001). The cofactor was parameterized both in the active form, PAPS, and in the inactive form, PAP. Force field parameters are available in the Supplementary Material. Simulations were performed with both forms of the cofactor and the results were compared. After having established that the PAP- and PAPS-containing simulations displayed similar results, PAP was chosen as the preferred cofactor, to stay close to the crystal structure complexes. 10 simulations of 1 ns,

starting from the same coordinates but using different random starting velocities, were performed for E2, OHP, E1, diethylstilbestrol (DES) and dienestrol (DIS) in complex with the PAP-bound dimeric form of hSULT1E1 as well as the PAP-bound mSULT1E1 monomer. To study the impact of dimerization of the human enzyme, 10 simulations were similarly performed for the monomeric form (chain A) of hSULT1E1 in complex with E2. To study the impact of crystal contacts in the hSULT1E1 structure, a 1 ns simulation of the periodic unit cell of the crystal structure, containing two dimers, was performed. All simulations were performed using the following protocol. Polar and aromatic hydrogen atoms were added to the protein-ligand complexes. The complexes were subsequently minimized and centred in a periodic box solvated with SPC water molecules (Berendsen 1981). The minimal solute-to-wall distance was 0.9 nm. The systems contained approximately 13.000 molecules (monomer), 21.000 molecules (dimer) and 8.300 molecules (crystal). 2 (mSULT1E1), 7 (hSULT1E1, monomer) and 14 (hSULT1E1, dimer) counterions (Na^+) were added at random positions to obtain a system with a net charge of zero. After another round of energy minimization, initial velocities were randomly assigned according to a Maxwell–Boltzmann distribution at 50 K. The systems were heated up gradually, increasing the temperature by 50 K every 20 ps, followed by 40 ps of equilibration at 298 K. During the heating up of the system, position restraints with an initial force constant of 2.5 10^4 kJ mol^{-1} nm^{-2} on the heavy atoms were gradually reduced by a factor 10 every 20 ps. Subsequently, 1 ns of simulation was performed. For some of the systems extended simulations were carried out to further study their dynamic behaviour. A time-step of 2 fs was used and all bonds were constrained using the SHAKE algorithm (Ryckaert 1977). All simulations were conducted at constant temperature and pressure, using the weak coupling algorithm (Berendsen 1984). The solute and solvent molecules were separately coupled to two temperature baths at 298 K with a relaxation time of 0.1 ps. The relaxation time for the isotropic pressure scaling was set to 0.3

ps with an isothermal compressibility of $2.807*10^{-5}$ atm^{-1} and a reference pressure of 1 atm. Non-bonded interactions were calculated using a triple range cutoff scheme. All interactions within 0.8 nm were calculated every time-step using a pair-list generated every fifth time-step. Long-range interactions, up to 1.4 nm, were calculated every fifth time-step. A reaction-field term was added to the energies and forces, with an effective dielectric constant of 61.0 to represent the electrostatic interactions outside the 1.4 nm cut-off (Tironi 1995). Coordinates were stored every 0.4 ps for the solute. All trajectories were analyzed using the GROMOS05 (Christen 2005) and GROMACS (Berendsen 1995; Lindahl 2001) biomolecular simulation packages.

3 Results

3.1. Validation of the mSULT1E1 inhibition assay

HPLC analysis confirmed the production of pyrene 1-sulfate from OHP in the presence of mSULT1E1, as described previously (Reinen 2006). The protein- and time-dependent formation of pyrene 1-sulfate from OHP was investigated. The formation of pyrene 1-sulfate by mSULT1E1 is linear (R^2 = 0.99) with increasing protein concentration up to 94 ng/ml. The formation of pyrene 1-sulfate by mSULT1E1 at a protein concentration of 25 ng/ml was linear in time for at least 30 min (R^2 = 0.97). See Figure S1 in the supplementary materials. The sulfo-conjugation of OHP by mSULT1E1 displayed typical Michaelis-Menten kinetics (R^2 = 0.98), see Figure S2. Apparent K_m and V_{max} values measured by the HPLC assay were 305 ± 31 nM and 140 ± 6 pmol/min/μg mSULT1E1 (means ± SD), respectively. No substrate inhibition could be observed within the tested range of substrate concentrations (up to 1 μM).

3.2. mSULT1E1 and hSULT1E1 inhibition screening and IC_{50} measurements

In order to identify mSULT1E1 inhibitors, a selection of 34 known EDCs, see Figure 3, was screened at a 2.5 μM concentration using the optimized mSULT1E1 inhibition assay conditions. Compounds were considered to be strong inhibitors when more than 50% inhibition of mSULT1E1 was observed at an inhibitor concentration of 2.5 μM. 8 strong inhibitors were identified. E1, 17α-estradiol (αE2), E2, 17α-ethinylestradiol (EE2) and estriol (E3) were found to be very strong inhibitors displaying more than 95% inhibition. DES, 11-HMBP and 4-HEP were found to be strong inhibitors.

15 compounds of the library of tested EDCs had not been screened previously in the hSULT1E1 inhibition assay.(Reinen 2006) These compounds were screened for hSULT1E1 inhibition and 4 strong inhibitors were identified; 4-HEP, daidzein, resveratrol and enterolactone, as displayed in Figure 3.

DIS (72%), enterolactone (62%), zearalenone (58%), genistein (52%), resveratrol (46%), hexestrol (31%), 4-HEP (30%) and progesterone (25%) showed stronger inhibition for hSULT1E1 than for mSULT1E1. Testosterone and 6-HEBP displayed stronger inhibition for mSULT1E1 than for hSULT1E1, with differences of 38 and 29% respectively. For all the other compounds the inhibition difference between the species was less than 25%.

Based on the inhibition screening and species differences results, 14 out of the 34 EDCs, listed in Table 1, were selected for IC_{50} measurements using the optimized mSULT1E1 inhibition assay. IC_{50} values using the hSULT1E1 inhibition assay for testosterone, progesterone, resveratrol and enterolactone were measured as well. The results are displayed in Table 2. Using the IC_{50} values, the K_i values and the ratio between the mSULT1E1 K_i and the hSULT1E1 K_i values were calculated, using the Cheng-Prusoff equation.(Cheng 1973) From Table 2 it can be concluded that there are significant differences between the binding affinities of E1, DIS and enterolactone between mSULT1E1 and hSULT1E1, all of these compounds being weaker binders of mSULT1E1. A significant difference in binding affinity is here defined as a ratio of K_i values significantly greater than 10. E1 and E2 both display similar binding affinities to mSULT1E1 as well as to hSULT1E1, which is in accordance with previous studies (Falany 1997; Hempel 2000; Song 2001). The difference in binding affinity of E1 originates from a slightly improved affinity for the human

protein and a slightly decreased affinity for the murine protein when compared to estradiol. However, the changes in affinity between E2 and E1 in one protein are less than a power of ten. Interestingly, DIS, which is structurally very similar to DES, displays a similar binding affinity as DES to hSULT1E1, whereas DIS is a significantly weaker binder than DES in mSULT1E1. Enterolactone is a very weak binder of mSULT1E1, whereas it is a reasonably strong binder of hSULT1E1.

However, even for the significant differences in affinity, the differences are not large enough to realistically be able to rationalize them computationally. Therefore, the focus of the computational work remained on general structural and mechanistic differences between the murine and human enzymes.

3.3 Computer modelling

3.3.1 General structural observations

The sequence identity of mSULT1E1 and hSULT1E1 is 77% and overall the structures are very similar. A comparison reveals a conserved region, both in terms of sequence and conformation, near the cofactor and a more variable region on the opposite side of the binding site, near the surface of the protein. Figure 4 displays the active site of the human E2-bound structure superposed on the murine E2-bound structure (1AQU) (Kakuta 1997). All amino acids in the active site that differ between the two proteins are displayed. A difference in the inner parts of the binding site is the substitution of Phe80 in hSULT1E1 for Tyr81 in mSULT1E1. This structural difference has been shown to be important for substrate specificity, by acting as a gate, preventing bulkier substrates, such as dehydroepiandrosterone

(DHEA) to be sulfonated by mSULT1E1 (Petrotchenko 1999). In the outer part of the binding site, the 17β-OH of E2 can form a hydrogen bond with Asn86 in mSULT1E1. In hSULT1E1 this position is occupied by Lys85, which in turn forms a salt bridge with Asp22, as displayed in Figure 4. Lys85 is pointing away from the binding site in the human apo-structure, but it displays significant flexibility both in terms of B-factors in crystal structures and during molecular dynamics simulations (Shevtsov 2003). In addition, mutagenesis studies have shown that Lys85 is not crucial for hSULT1E1 E2 sulfonation (Hempel 2000). Similar to hSULT1E1, mSULT1E1 also has two residues that form a salt bridge on this side of the binding site, but in a slightly shifted position; Arg23 and Asp21, corresponding to Asp22 and Tyr20 in hSULT1E1. In addition to these salt-bridge pairs, hSULT1E1 displays Lys10 located further away from the substrate The corresponding residue in mSULT1E1 is Val11. Another difference between the mSULT1E1 and the hSULT1E1 structures is in the loop containing residues 146-148 (hSULT1E1 numbering). The residues in this loop differ between hSULT1E1 and mSULT1E1, being more hydrophilic in the murine structure, see Figure 4 for details. Moreover, on position 142 (hSULT1E1 numbering) the Phe of hSULT1E1 is substituted for a Leu in mSULT1E1. In summary, hSULT1E1 has more aromatic and hydrophobic residues than mSULT1E1 in the buried parts of the binding site.

3.3.2 Molecular dynamics simulations of E2 in hSULT1E1 and mSULT1E1

Molecular dynamics simulations were initially performed for E2 bound to solvated mouse and human SULT1E1 in complex with PAPS, starting from the crystal structures. Surprisingly, the substrate moved away from the catalytically active position at different times during the simulations. Different parameters, e.g. different ionization states, of the cofactor were tested, as well as performing the simulations with inactive cofactor PAP. In addition,

different restraints were applied during the equilibration of the simulations and the simulation time was extended to up to 4 ns. However, the substrate still moved away from the catalytically active position observed in the crystal structures. A similar observation was made by Gorokhov *et al* when simulating heparan sulfate N-sulfotransferase (Gorokhov 2000). Heparan sulfate N-sulfotransferase is not a cytosolic sulfotransferase and the catalytic histidine residue is substituted by a glutamate, most likely acting as a catalytic base. Gorokhov *et al* did not observe a direct hydrogen bond between the substrate and the catalytic base during the simulation. Instead water-bridged hydrogen bonds were observed (Gorokhov 2000). Such movements were not observed in a previous QM/MM study on similar complexes, but these simulations included only very limited dynamics at maximally 200 K and with distance constraints between the substrate and the active site residues (Lin 2006).

To investigate whether the observed effect was due to a simulation defect or a result of simulating the proteins free in solution as opposed to in a crystal, a crystal simulation was performed for hSULT1E1. Interestingly, the movement of the substrates in the crystal were significantly less than in the simulations of the proteins free in solution. Table 3 displays the percentage of time of the simulation in which the 3-hydroxyl oxygen of E2 is within 3.5 Å of His107Nε and the RMS deviation of the substrate atoms during the simulation. The corresponding values for the simulations of the human dimer in solution are also displayed in Table 3. The substrate is not forming a hydrogen bond with His107 during the simulation in any of the monomers in the crystal. However, the movement of the substrate is very small, with a total RMS deviation of only 1.2 Å, and this deviation is fairly constant over time, indicating that the substrate moves away only slightly from its initial position as observed in the crystal structure. In the dimer simulations the substrate displays more movement than in the crystal, as can be seen from the RMS deviation values. Note that the values for the dimer

are averages over 10 simulations, whereas the crystal simulation was only performed once, and the values are an average over the 2 identical monomers in the simulated unit cell.

To study which parts of the protein were more flexible in the simulation of the dimer free in solution as compared to the crystal, the RMS fluctuations of the backbone of the protein were monitored. The parts of the protein that fluctuate more in the simulation of the free dimer are residues 1-20, 60-70, 110-120 and 215-230. The residues near the N-terminal as well as residues 215-230 could have direct influence on the shape and interactions of part of the active site.

3.3.3 Studies of the dimerization interface and the importance of the quaternary structure for substrate positioning and interactions in the active site

Most cytosolic sulfotransferases, with the exception of mSULT1E1, are homodimers. The dimerization interface has been identified to be a short segment at the carboxyl terminus, containing the KXXXTVXXXE sequence. Mutation of the valine in this sequence to a glutamate has been shown to result in monomer formation and introducing this sequence in naturally occurring sulfotransferase monomers converts them to dimers (Petrotchenko 2001). Although Zhang *et al* have argued that one of the active sites in the dimer functions as an allosteric site, which could be an explanation for substrate inhibition, several studies show that total activity and substrate inhibition is independent of subunit dimerization (Zhang 1998). The same has also been observed for substrate affinity (Petrotchenko 2001; Pedersen 2002; Lu 2008; Lu 2009). Lu *et al* suggest that the main role for dimerization of sulfotransferases could be to maintain structural stability (Lu 2009).

The E2-containing hSULT1E1 structure crystallizes as a homodimer, but contains the V269E mutation which disrupts the dimer in solution. Simulations were made using this structure as well as one of the monomers of the hSULT1E1 and results of the ligand positioning and interactions were compared (Table 4). It can be seen that the dimer and monomer simulations behave very similarly in terms of substrate interaction with His107 throughout the simulations. The RMS deviation of the substrate is somewhat higher in the monomer simulations than in the dimer ones. These results indicate that the time the substrate stays in the catalytic position is similar in the monomer and the dimer simulations, but when the substrate moves, it moves slightly more in the monomer than in the dimer. Note that the results are average values over 10 simulations. No significant differences were observed between the RMS fluctuations of the backbone atoms in the simulations of the dimer and the monomer. Differences in the fluctuations of side-chain atoms of active site residues were observed for Tyr20 and Lys85, which displayed larger average fluctuations in the monomer simulations.

To study the stability of the human monomer in solution compared to the dimer, as well as the stability of the dimer in solution, the secondary structure was monitored during the simulations. The dimer displayed stable secondary structure during the simulations. Differences between the monomer and the dimer simulations were observed for the helix consisting of residues 64-69 on the surface of the protein and for the helix consisting of residues 261-264, leading up to the dimer interface, see Figure 5. These helices appeared to be less stable in the monomer simulation.

These results in combination with the previously reported results for SULT1E1 and other sulfotransferases, where no difference between natural dimers or mutated monomers

could be found for substrate activity or substrate inhibition, leads us to believe that the substrate interactions and positioning in the active site is not a direct result of the quaternary structure of the protein.

The interactions between the monomers at the dimer interface were studied in more detail. In the wild-type hSULT1E1 structure, PDB code 1G3M (Shevtsov 2003), there are 6 hydrogen bonds between the monomers; Lys264O(A)–Ala270H(B), Phe267O(A)–Val269H(B), Lys264NZ(A)-Glu273OE2(B) and the inverse for the other monomer. In the simulations both the hydrogen bonds between Lys264 and Glu273 are completely disrupted, in accordance with the crystal structure of the V269E mutant, see Figure 5 for details. Moreover, during the course of the simulations water molecules enter the interface and some of the direct hydrogen bonds are substituted with interactions with water, bridging the interactions between the monomers. The distance between the monomers was measured in simulations of each of the following ligands bound to hSULT1E1: E2, E1, OHP, DES and DIS. Figure 6 displays the distance between the monomers, calculated as the distance between the centres of geometry of the α-carbons of the backbone of residues 264-273 of the two monomers, averaged over 10 1 ns simulations. The distance increases from 6.5 Å initially up to 9.5 Å at the end of the simulations and is continuously increasing. The same distance in the crystal simulation stays around 6.5 Å throughout the simulation. Note that the simulation times are too short for any significant structural changes to occur, as confirmed by the conserved secondary structure throughout the dimer simulations. However, it seems that the initial stages of monomerization of the SULT1E1 V269E mutant can be observed.

3.3.4 Differences between mSULT1E1 and hSULT1E1

Based on the experimental inhibition data, 5 compounds were simulated in complex with both murine and human SULT1E1; E2, E1, DES, DIS and the substrate used in the enzyme assay, OHP. All simulations were performed 10 times for 1 ns in each protein. The ligands were first positioned in a position compatible with catalytic activity. However, all five ligands moved away from this position in a number of simulations. Table 5 displays the average occurrence of a hydrogen bond between the hydroxyl-group of the ligand and His107Nε as well as the average RMS deviation of the ligand atoms. With the exception of OHP, the compounds stay on average longer in the catalytic pose in the murine protein. To study whether the movements of the ligands are similar in the murine and human proteins, the average fluctuations of the atoms of E2 were calculated. As displayed in Figure 7, the fluctuation pattern is similar for all simulation conditions with the exception of mSULT1E1. E2 displays more equal fluctuations throughout the molecule in the murine protein, whereas the ligand atom fluctuations in the human protein show a minimum in the middle of the molecule, indicating a "twisting" movement around the centre of the molecule. The average fluctuations are smaller in the murine protein, suggesting that it stays in a more stable position for a longer period of time than the ligand in the human protein. Table 5 also shows the percentage of the simulations where the catalytically important hydrogen bond is present for more than 50% of the simulation.

The hydrogen bonds between the other oxygen of the ligand and Asp22/Lys85 (hSULT1E1) and Arg23/Asn86 (mSULT1E1) on the opposite side of the binding pocket were also monitored and are displayed in Table 5. For DES and DIS in hSULT1E1 the hydrogen bond with His107 is substituted by hydrogen bonds with Asp22 and Lys85, whereas for the other ligands and for the murine protein simulations it is less clear if that is the case. In order to determine whether it would be possible for the ligands to form hydrogen bonds with the two oxygen/hydroxyl-groups and the protein simultaneously, the distances between

His107/108Nε on one side of the binding pocket and Asp21Cγ(human)/Arg22Cζ(murine) as well as Lys84Nζ(human)/Asn85Cγ(murine) were monitored during the simulations (table 5). The distances between the two oxygen atoms in the ligands (e.g. 3-OH and 17-OH for E2) were also monitored. The shortest distance in mSULT1E1 is approximately 13.5 Å in all simulations, whereas the shortest distance in hSULT1E1 is 15.2 Å. The ligand O-O distance is similar in the mSULT1E1 and hSULT1E1 simulations. It can be expected that E2 and E1 will not form the two hydrogen bonds simultaneously in the human protein, whereas this could be possible in the murine protein. For DES and DIS that display a longer distance between the two oxygens, these hydrogen bonds could be formed simultaneously in both the human and murine proteins. The percentage of simulations in which ligand-protein hydrogen bonds at both sides of the binding pocket are observed simultaneously (table 5), is significantly higher in mSULT1E1 than in the human protein. As expected, in the human protein it is mostly for DES and DIS that both hydrogen bonds occur.

Experimentally, E2 displays similar affinity to hSULT1E1 and mSULT1E1. However, the substrate stays longer in the catalytic position in the murine protein. The trajectories of the simulations show that the substrate in the hSULT1E1 simulations moves away from the active site to a position where it can form hydrogen bonds with Asp22 and Lys85. This part of the pocket also offers a hydrophobic environment for the rest of the substrate, more so than in the murine protein. Figure 8 displays the last snapshots of 10 simulations of E2 in hSULT1E1 and mSULT1E1. More substrates are still located in the catalytically active position in the murine protein simulations, whereas those substrates that have left this position are fairly spread over the binding pocket. In contrast, fewer substrates are located in the catalytically active position in hSULT1E1. Moreover, the substrates in a different position than the catalytically active ones seem to gather in one sub-pocket of the active site, offering hydrophobic interactions as

well as hydrogen bond opportunities with Asp22 and Lys85. Similar behaviour was observed for the other ligands simulated in this study.

DES is a substrate for both human and murine SULT1E1, but displays a significantly lower activity in the human protein (Falany 1997; Kakuta 1998a). However, the inhibition of both enzymes by DES is similar, as displayed in Table 2. The existence of a second binding site/binding pose within the active site of hSULT1E1 could explain this observation. The 10-fold longer time that DES stays in the catalytic position in the murine protein and the high percentage of hydrogen bond formation with Asp22 and Lys85 in the human protein all point to the substrate moving away quickly from the catalytically active position in hSULT1E1 to a second, catalytically inactive, binding site displaying a similar or stronger binding affinity.

DIS is not a substrate for bovine SULT1E1, but has to our knowledge not been tested in murine or human SULT1E1. DIS and DES display similar affinity to the human protein, see Table 2, but the affinity of DIS in mSULT1E1 is 30 times weaker than that of DES. No direct reason for this could be suggested from the data in Table 5.

In summary, the ligands in the murine protein stay longer in the catalytically active pose during the simulations than in the human protein. This is most probably a result of the opportunity to form hydrogen bonds on both sides of the active site in mSULT1E1, which is not possible to the same extent in hSULT1E1. The ligands in hSULT1E1 seem to move to a sub-pocket, offering hydrophobic interactions as well as possibilities to form hydrogen bonds with Asp22 and Lys85. In mSULT1E1 the movement is more random after the substrate has left the catalytically active pose. It is possible that the human protein offers two distinct binding sites, whereas the murine protein only has one. This offers an explanation to the more favourable binding affinity for the human protein of the ligands tested in this study as well as a possible explanation to substrate inhibition observed in hSULT1E1, but not in mSULT1E1.

4 Discussion

The aim of this study was to investigate the differences in inhibition by EDCs of murine and human estrogen sulfotransferase *in vitro* and *in silico* and to study whether the observed differences could give suggestions as to reasons for differences in substrate inhibition and quaternary structure of these two proteins.

Human SULT1E1 displays substrate inhibition at higher concentrations of different substrates (Falany 1995; Reinen 2006), whereas no substrate inhibition has been observed for murine SULT1E1.(Kakuta 1998a) This was confirmed here for OHP, as no substrate inhibition was observed in murine SULT1E1 in the concentration range tested. This again indicates that the OHP-assay is very similar to an estradiol-based assay, with the significant difference that no radio-active compounds are required to perform the experiments (Reinen 2006).

Based on the inhibition screening results of 34 EDCs and the previously determined IC_{50} values for hSULT1E1, 14 EDCs were selected for IC_{50} value measurements. The binding affinities (K_i values) were similar for most of the compounds, except for E1, DIS and enterolactone, which displayed 20 to 50 times higher affinity for hSULT1E1. Large similarities between the two enzymes with regards to the bioactivation of a large set of SULT-dependent promutagens have also been found previously (H.R. Glatt, unpublished results). The selection of 34 EDCs that were screened includes five structurally related polycyclic compounds which were bioactivated to mutagens by hSULT1E1 and mSULT1E1 at up to 200-fold different levels (H.R. Glatt, unpublished results). Interestingly, only small differences were observed in affinity for human and murine SULT1E1 for these compounds.

Comparison of the murine and human SULT1E1 structures suggests that their binding sites are very similar. Differences involve differences in hydrogen bond-forming residues in the outer part of the binding site as well as a larger amount of hydrophobic and aromatic residues in the buried part of the binding site of the human SULT1E1 structure.

In the simulations of the natural substrate, E2, in complex with both PAPS- and PAP-bound hSULT1E1 and mSULT1E1, the substrate moved away from the catalytically active position, observed in the crystal structures. Interestingly, the substrate movement in the simulation of a unit cell of the hSULT1E1 crystal structure was significantly less, indicating that the substrate movement in the proteins free in solution is not a simulation defect. Differences in movement of the backbone in the free and crystal simulations were observed and included two regions close to the binding site, residues 1-20 and 215-230. Pedersen *et al* observed that crystal contacts in the structure of SULT2A3 could be the reason that the substrate, DHEA, was unable to bind to the protein, although the crystal was soaked with high concentrations of the substrate (Pedersen 2000). They observed that considerable differences in the conformations of residues 18-23, 82-90 and 239-252 (hSULTE1 numbering) exist between human SULT2A3 and mSULT1E1 and that e.g. the loop of the corresponding residues 239-252 in SULT2A3 would have to change conformation in order to accommodate DHEA in a similar orientation as E2 in mSULT1E1. A number of substrate/inhibitor bound sulfotransferase crystal structures are the result of crystal soaking experiments (Kakuta 1997; Kakuta 1998b; Pedersen 2000; Pedersen 2002; Shevtsov 2003), which will likely not allow for large conformational changes to occur upon ligand binding. Interestingly, some substrate-bound crystal structures that are the result of co-crystallization experiments display either multiple ligands in the binding site or several possible orientations of the ligand (Rehse 2002;

Gamage 2003; Gamage 2005). In combination with ligand movements observed during the present simulations, this suggests that there are several favourable binding poses in sulfotransferases, possibly not observed in the ligand soaked crystal structures. Multiple binding orientations in the active site, one of them catalytically inactive, has also been suggested to explain substrate inhibition at higher substrate concentrations. When the inactive binding orientation becomes more occupied at higher substrate concentrations this may block the substrate from binding in the catalytically active pose.

Similarly to many other cytosolic sulfotransferases, hSULT1E1 has been shown to be biologically active as a dimer. In contrast, mSULT1E1 is active as a monomer. Zhang *et al* (Zhang 1998) proposed that one of the binding sites in the hSULT1E1 dimer is catalytic and the other site is allosteric and regulates turnover. However, it has also been shown that activity, affinity and substrate inhibition are independent of subunit dimerization (Petrotchenko 2001; Pedersen 2002; Lu 2008; Lu 2009). It has been suggested that the role of dimerization is to maintain structural stability (Lu 2009). The simulations performed in this study show no differences in ligand (E2) movement or interactions in the hSULT1E1 monomer and dimer. The secondary structure is maintained throughout the simulations of dimeric hSULT1E1. In contrast, the human monomer simulations display disruption of the secondary structure in helices on the surface and leading up to the dimer interface, confirming that dimerization could have an effect on structural stability.

The differences in ligand-protein interactions and ligand movements during the simulations of ligand-bound hSULT1E1 and mSULT1E1 were also studied. In general, the ligands stayed longer in their catalytically active position in mSULT1E1 than in hSULT1E1. Based on distance and hydrogen bond analysis we suggest that this observation is explained

by the ability of the ligands to form hydrogen bonds with both its hydroxyl-groups simultaneously in mSULT1E1, whereas this is not possible to the same extent in hSULT1E1. The movement of the ligands, when having moved away from the catalytically active position, is larger in the murine than in the human enzyme. Analysis of the trajectories of the simulations suggests that the ligands in the human protein move to a sub-pocket in the active site allowing for interaction with Asp22 and Lys85 as well as offering hydrophobic interactions. The movement of the ligands in the mSULT1E1 active site is more random. Lys85 has been shown not to be crucial for activity in hSULT1E1 (Hempel 2000). The K_m for E2, E1 and DHEA even decreased slightly in the K85A mutant compared to the wild-type. Our *in silico* observations agree with these studies, as we are proposing a second non-catalytic binding pose in the active site possibly made less favourable due to the mutation. A similar effect was observed for the corresponding mSULT1E1 mutant, N86A (Petrotchenko 1999). As the activities of E2 in hSULT1E1 and mSULT1E1 are similar, we do not suggest that the ability of this ligand to form hydrogen bonds on both sides of the binding pocket simultaneously is affecting activity, but merely the affinity of the ligands in the catalytically active position. Additional favourable binding orientations for some ligands in hSULT1E1 would offer an explanation of why DES shows significantly lower activity in hSULT1E1 than in mSULT1E1, but displays similar binding affinities to the two proteins. Our simulations suggest that DES moves away very quickly from the catalytically active pose in hSULT1E1, whereas it stays significantly longer in mSULT1E1. A favourable second binding pose in hSULT1E1 would explain the similar binding affinities in hSULT1E1 and mSULT1E1. The substrate OHP, which has only one hydrogen bonding moiety, is the only compound that behaves similarly in the two proteins. However, the activity for this substrate is almost 50 times lower in mSULT1E1 compared to hSULT1E1.

PAP has been shown to be a strong inhibitor of sulfotransferases, strengthening the hypothesis of substrate inhibition due to the formation of dead-end complexes (Rens-Domiano 1987; Zhang 1998). It is therefore surprising that mSULT1E1 does not seem to display substrate inhibition. However, murine SULT1E1 has been studied significantly less than hSULT1E1. It is possible that substrate inhibition and non-competitive inhibition is a combination of effects, both dead-end complex formation and a second favourable, but non-productive, binding orientation in the active site. More studies, e.g. mutations of the 85/86 and 22/23 positions in the hSULT1E1 and mSULT1E1 proteins and studies of substrate inhibition patterns in the mutants could shed more light on this issue.

Acknowledgements

The authors thank Prof. Negishi for making the 17β-estradiol/PAP SULT1E1 complex structure available.

Supplementary material

Figures S1 (dependency of OHP sulfo conjugation on protein concentration and on time) and S2 (Michaelis-Menten kinetics of OHP sulfo conjugation) as well as force-field parameters for cofactors PAP and PAPS are available in the supplementary material

5 References

Allali-Hassani, A., Pan, P. W., Dombrovski, L., Najmanovich, R., Tempel, W., Dong, A., Loppnau, P., Martin, F., Thonton, J., Edwards, A. M., Bochkarev, A., Plotnikov, A. N., Vedadi, M. and Arrowsmith, C. H., 2007. Structural and chemical profiling of the human cytosolic sulfotransferases. PLoS Biology 5, 1063-1078.

Barnett, A. C., Tsvetanov, S., Gamage, N. U., Martin, J. L., Duggleby, R. G. and McManus, M. E., 2004. Active site mutations and substrate inhibition in human sulfotransferase 1A1 and 1A3. J. Biol. Chem. 279, 18799-18805.

Berendsen, H. J. C., Postma, J. P. M., van Gunsteren, W. F., di Nola, A. and Haak, J. R., 1984. Molecular dynamics with coupling to an external bath. J. Chem. Phys. 81, 3684-3690.

Berendsen, H. J. C., Postma, J. P. M., van Gunsteren, W. F. and Hermans, J., 1981. Interaction models for water in relation to protein hydration. Intermolecular Forces. Dordrecht, The Netherlands, Reidel, 331-342.

Berendsen, H. J. C., van der Spoel, D. and van Drunen, R., 1995. GROMACS: A message-passing parallell molecular dynamics implementation. Comp. Phys. Comm. 91, 43-56.

Bolger, R., Wiese, T. E., Ervin, K., Nestich, S. and Checovich, W., 1998. Rapid screening of environmental chemicals for estrogen receptor binding capacity. Environ. Health. Perspect. 106, 551-557.

Chapman, E., Best, M. D., Hanson, S. R. and Wong, C.-H., 2004. Sulfotransferases: structure, mechanism, biological activity, inhibition, and synthetic utility. Angew. Chemie Int. Ed. 43.

Cheng, Y. and Prusoff, W. H., 1973. Relationship between the inhibition constant (K1) and the concentration of inhibitor which causes 50 per cent inhibition (I50) of an enzymatic reaction. Biochem. Pharmacol. 22, 3099-3108.

Christen, M., Hunenberger, P. H., Bakowies, D., Baron, R., Burgi, R., Geerke, D. P., Heinz, T. N., Kastenholz, M. A., Krautler, V., Oostenbrink, C., Peter, C., Trzesniak, D. and van Gunsteren, W. F., 2005. The GROMOS software for biomolecular simulation: GROMOS05. J. Comp. Chem. 26, 1719-51.

Cui, D., Booth-Genthe, C., Carlini, E., Carr, B. and Schrag, M. L., 2004. Heterotropic modulation of sulfotransferase 2A1 activity by celecoxib: product ratio switching of ethinylestradiol sulfation. Drug. Metab. Disp. 32, 1260-1264.

Falany, C. N., 1997. Enzymology of human cytosolic sulfotransferases FASEB J 11, 206-216.

Falany, C. N., Krasnykh, V. and Falany, J. L., 1995. Bacterial expression and characterization of a cDNA for human liver estrogen sulfotransferase. J. Steroid Biochem. Mol. Biol. 52, 529-539.

Gamage, N. U., Duggleby, R. G., Barnett, A. C., Tresillian, M., Latham, C. F., Liyou, N. E., McManus, M. E. and Martin, J. L., 2003. Structure of human carcinogen-converting enzyme SULT1A1. Structural and kinetic implications of substrate inhibition. J. Biol. Chem. 278, 7655-7662.

Gamage, N. U., Tsvetanov, S., Duggleby, R. G., McManus, M. E. and Martin, J. L., 2005. The structure of human SULT1A1 crystallized with estradiol. An insight into active site plasticity and substrate inhibition with mult-ring substrates J. Biol. Chem. 280, 41482-41486.

Glatt, H., Bartsch, I., Czich, A., Seidel, A. and Falany, C. N., 1995a. Salmonella strains and mammalian cells genetically engineered for expression of sulfotransferases. Toxicol. Lett. 82-83, 829-834.

Glatt, H. and Meinl, W., 2004. Pharmacogenetics of soluble sulfotransferases (SULTs). Naunyn Schmiedeberg's Arch. Pharmacol. 369, 55-68.

Glatt, H., Pauly, K., Czich, A., Falany, J. L. and Falany, C. N., 1995b. Activation of benzylic alcohols to mutagens by rat and human sulfotransferases expressed in Escherichia coli. Eur. J. Pharmacol. 293, 173-181.

Gorokhov, A., Perera, L., Darden, T. A., Negishi, M., Pedersen, L. C. and Pedersen, L. G., 2000. Heparan sulfate biosynthesis: a theoretical study of the initial sulfation step by N-deacetylase/N-sulfotransferase Biophys. J. 79, 2909-2917.

Harris, R. M., Wood, D. M., Bottomley, L., Blagg, S., Owen, K., Hughes, P. J., Waring, R. H. and Kirk, C. J., 2004. Phytoestrogens are potent inhibitors of estrogen sulfation: implications for breast cancer risk and treatment. J. Clin. Endocrin. Metab. 89, 1779-1787.

Hempel, N., Barnett, A. C., Bolton-Grob, R. M., Liyou, N. E. and McManus, M. E., 2000. Site-directed mutagenesis of the substrate-binding cleft of human estrogen sulfotransferase. Biochem. Biophys. Res. Commun. 276, 224-230.

Hoff, R. H., Czyryca, P. G., Sun, M., Leyh, T. S. and Hengge, A. C., 2006. Transition state of the sulfyryl transfer reaction of estrogen sulfotransferase J. Biol. Chem. 281, 30645-30649.

Hotchkiss, A. K., Rider, C. V., Blystone, C. R., Wilson, V. S., Hartig, P. C., Ankley, G. T., Foster, P. M., Gray, C. L. and Gray, L. E., 2008. Fifteen years after "Wingspread"--environmental endocrine disrupters and human and wildlife health: where we are today and where we need to go. Toxicol. Sci. 105, 235-259.

Jones, G., Willett, P., Glen, R. C., Leach, A. R. and Taylor, R., 1997. Development and validation of a genetic algorithm for flexible docking. J. Mol. Biol. 267, 727-748.

Kakuta, Y., Pedersen, L. C., Chae, K., Song, W.-C., Leblanc, D., London, R., Carter, C. W. and Negishi, M., 1998a. Mouse steroid sulfotransferases. Substrate specificty and preliminary x-ray crystallographic analysis. Biochem. Pharmacol. 55, 313-317.

Kakuta, Y., Pedersen, L. G., Carter, C. W., Negishi, M. and Pedersen, L. C., 1997. Crystal structure of estrogen sulphotransferase. Nat. Struct. Biol. 4, 904-908.

Kakuta, Y., Petrotchenko, E. V., Pedersen, L. C. and Negishi, M., 1998b. The sulfuryl transfer mechanism. Crystal structure of a vanadate complex of estrogen sulfotransferase and mutational analysis. J. Biol. Chem. 273, 27325-27330.

Kester, M. H. A., Bulduk, S., Tibboel, D., Meinl, W., Glatt, H., Falany, C. N., Coughtrie, M. W. H., Bergman, A., Safe, S. H., Kuiper, G. G. J. M., Schuur, A. G., Brouwer, A. and Visser, T. J., 2000. Potent inhibition of estrogen sulfotransferase by hydroxylated PCB metabolites: a novel pathway for explaining the estrogenic activity of PCBs. Endocrinology 141, 1897-1900.

Kester, M. H. A., Bulduk, S., van Toor, H., Tibboel, D., Meinl, W., Glatt, H., Falany, C. N., Coughtrie, M. W. H., Schuur, A. G., Brouwer, A. and Visser, T. J., 2002. Potent inhibition of estrogen sulfotransferase by hydroxylated metabolites of polyhalogenated aromatic hydrocarbons reveals alternative mechanism for estrogenic activity of endocrine disruptors. J. Clin. Endocrin. Metab. 87, 1142-1150.

Lee, K. A., Fuda, H., Lee, Y. C., Negishi, M., Strott, C. A. and Pedersen, L. C., 2003. Crystal structure of human cholesterol sulfotransferase (SULT2B1b) in the presence of pregnenolone and 3'-phosphoadenosin 5'-phosphate. J. Biol. Chem. 278, 44593-44599.

Lin, P, Yang, W., Pedersen, L.C., Negishi, M, Pedersen, L.G. 2006. Searching for the minimum energy path in the sulfuryl transfer reaction catalyzed by human estrogen sulfotransferase: role of enzyme dynamics. Int. J. Quant. Chem. 106, 2981-2998.

Lindahl, E., Hess, B. and van der Spoel, D., 2001. GROMACS 3.0: A package for molecular simulation and trajectory analysis. J. Mol. Mod. 7, 306-317.

Lu, L.-Y., Chiang, H.-P., Chen, W.-T. and Yang, Y.-S., 2009. Dimerization is responsible for the structural stability of human sulfotransferase 1A1. Drug. Metab. Disp. 37, 1083-1088.

Lu, L.-Y., Hsieh, Y.-C., Liu, M.-Y., Lin, Y.-H., Chen, C.-J. and Yang, Y.-S., 2008. Identification and characterization of two amino acids critical for the substrate inhibition of human dehydroepiandrosterone sulfotransferase (SULT2A1). Mol. Pharmacol. 73, 660-668.

Ma, B., Shou, M. and Schrag, M. L., 2003. Solvent effect on cDNA-expressed human sulfotransferase (SULT) activities in vitro. Drug. Metab. Disp. 31, 1300-1305.

MOE, Molecular operating environment, version 2008.10, Chemical Computing Group Inc. Montreal, Quebec, Canada.

Negishi, M., Pedersen, L. G., Petrotchenko, E., Shevtsov, S., Gorokhov, A., Kakuta, Y. and Pedersen, L. C., 2001. Structure and function of sulfotransferases. Arch. Biochem. Biophys. 390, 149-157.

Pedersen, L. C., Petrotchenko, E., Shevtsov, S. and Negishi, M., 2002. Crystal structure of the human estrogen sulfotransferase-PAPS complex: evidence for catalytic role of Ser137 in the sulfuryl transfer reaction. J. Biol. Chem. 277, 17928-17932.

Pedersen, L. C., Petrotchenko, E. V. and Negishi, M., 2000. Crystal structure of SULT2A3, human hydroxysteroid sulfotransferase. FEBS Lett. 475, 61-64.

Petrotchenko, E., Doerflein, M. E., Kakuta, Y., Pedersen, L. C. and Negishi, M., 1999. Substrate gating confers steroid specificity to estrogen sulfotransferase. J. Biol. Chem. 274, 30019-30022.

Petrotchenko, E. V., Pedersen, L. C., Borchers, C. H., Tomer, K. B. and Negishi, M., 2001. The dimerization motif of cytosolic sulfotransferases. FEBS Lett. 490, 39-43.

Qian, Y., Deng, C. and Song, W. C., 1998. Expression of estrogen sulfotransferase in MCF-7 cells by cDNA transfection suppresses the estrogen response: potential role of the enzyme in regulating estrogen-dependent growth of breast epithelial cells. J. Pharmacol. Exp. Ther. 286, 555-560.

Qian, Y. and Song, W.-C., 1999. Correlation between PAP-dependent steroid binding activity and substrate specificity of mouse and human estrogen sulfotransferases. J. Steroid Biochem. Mol. Biol. 71, 123-131.

Rehse, P. H., Zhou, M. and Lin, S.-X., 2002. Crystal structure of human dehydroepiandrosterone sulphotransferase in complex with substrate. Biochem. J. 364, 165-171.

Reinen, J., Vriese, E., Glatt, H. and Vermeulen, N. P., 2006. Development and validation of a fluorescence HPLC-based screening assay for inhibition of human estrogen sulfotransferase. Anal. Biochem. 357, 85-92.

Rens-Domiano, S. S. and Roth, J. A., 1987. Inhibition of M and P phenol sulfotransferase by analogues of 3'-phosphoadenosine-5'-phosphosulfate. J. Neurochem. 48, 1411-1415.

Ropero, A. B., Alonso-Magdalena, P., Ripoll, C., Fuentes, E. and Nadal, A., 2006. Rapid endocrine disruption: environmental estrogen actions triggered outside the nucleus. J. Steroid Biochem. Mol. Biol. 102, 163-169.

Ryckaert, J.-P., Ciccotti, G. and Berendsen, H. J. C., 1977. Numerical integration of cartesian equations of motion of a system with constraints: Molecular dynamics of n-alkanes. J. Comput. Phys. 23, 327-341.

Schuler, L. D., Daura, X. and van Gunsteren, W. F., 2001. An improved GROMOS96 force field for aliphatic hydrocarbons in the condensed phase. J. Comp. Chem. 22, 1205-1218.

Shevtsov, S., Petrotchenko, E. V., Pedersen, L. C. and Negishi, M., 2003. Crystallographic analysis of a hydroxylated polychlorinated biphenyl (OH-PCB) bound to the catalytic estrogen binding site of human estrogen sulfotransferase. Environ. Health. Perspect. 111, 884-888.

Song, W. C., 2001. Biochemistry and reproductive endocrinology of estrogen sulfotransferase. Ann. NY Acad. Sci. 948, 43-50.

Song, W. C. and Melner, M. H., 2000. Steroid transformation enzymes as critical regulators of steroid action in vivo. Endocrinology 141, 1587-1589.

Strott, C. A., 1996. Steroid sulfotransferases. Endocrine Rev. 17, 670-697.

Suzuki, T., Miki, Y., Nakata, T., Shiotsu, Y., Akinaga, S., Inoue, K., Ishida, T., Kimura, M., Moriya, T. and Sasano, H., 2003. Steroid sulfatase and estrogen sulfotransferase in normal human tissue and breast carcinoma. J. Steroid Biochem. Mol. Biol. 86, 449-454.

Teramoto, T., Sakakibara, Y., Liu, M.-C., Suiko, M., Kimura, M. and Kakuta, Y., 2009. Snapshot of a Michaelis complex in a sulfuryl transfer reaction: Crystal structure of a mouse sulfotransferase, mSULT1D1, complexed with donor substrate and acceptor substrate. Biochem. Biophys. Res. Commun. 383.

Tironi, I. G., Sperb, R., Smith, P. E. and van Gunsteren, W. F., 1995. A generalized reaction field method for molecular-dynamics simulations. J. Chem. Phys. 102, 5451-5459.

Tyapochkin, E., Cook, P. F. and Chen, G., 2008. Isotope exchange at equilibrium indicates a steady state ordered kinetic mechanism for human sulfotransferase. Biochemistry 47, 11894-11899.

Utsunomiya, H., Ito, K., Suzuki, T., Kitamura, T., Kaneko, C., Nakata, T., Niikura, H., Okamura, K., Yaegashi, N. and Sasano, H., 2004. Steroid sulfatase and estrogen sulfotransferase in human endometrial carcinoma. Clin. Cancer Res. 10, 5850-5856.

Zhang, H., Varmalova, O., Vargas, F. M., Falany, C. N. and Leyh, T. S., 1998. Sulfuryl transfer: the catalytic mechanism of human estrogen sulfotransferase J. Biol. Chem. 273, 10888-10892.

Figure 1. The reaction mechanism of sulfotransferases is proposed to be a sequential mechanism either of an ordered bi-bi (A) or a random bi-bi (B) character. The filled circles indicate the possible dead-end complexes in the two different types of mechanisms. SULT1E1 = estrogen sulfotransferase, PAPS = 3'-phosphoadenosine 5'-phosphosulfate (active cofactor), PAP = adenosine-3',5'-diphosphate (inactive cofactor), E2 = 17β-estradiol (substrate), E2S = 17β-estradiol-3-sulfate. Note that there are two more possible ways to reach each dead-end complex in (B). The SULT1E1-PAP-E2 complex can also be reached by PAP binding to the SULT1E1-E2 complex (top right) and the SULT1E1-PAPS-E2S complex can also be reached by E2S binding to the SULT1E1-PAPS complex. These are not shown in the figure as the renewed binding of either of the two reaction products (PAP and E2S) is considered to be much less probable, due to the much higher concentrations of PAPS and E2, respectively (under experimental conditions).

Figure 2. His107 accepts a proton form the hydroxyl group of the substrate, which can subsequently attack the S of the cofactor. The substrate is thought to be positioned in a catalytically favourable orientation through interaction with Lys105 and His107. Lys47, Lys105 and His107 can interact with the cofactor, stabilizing the transition state.

Figure 3. Inhibition screening of 34 compounds with known estrogenic properties. mSULT1E1 incubations (n = 3) were performed in the presence of 50 ng/ml enzyme, 250 nM 1-hydroxypyrene, and 2.5 µM inhibitor for 30 min at 37 °C at pH 7.4. hSULT1E1 incubations (n = 3) were performed in the presence of 4 ng/ml enzyme, 18.75 nM 1-hydroxypyrene, and 2.5 µM inhibitor for 30 min at 37 °C at pH 7.4. BP3, benzophenone-3; HCB, hexachlorobenzene; BPA, bisphenol A; 4-HEP, (±)-4-(α-hydroxyethyl)pyrene; 11-HMBP,

11-hydroxymethylbenzo[*a*]pyrene; 6-HEBP, (±)-6-(α-hydroxyethyl)benzo[*a*]pyrene; 6 HMBP, 6-hydroxymethylbenzo[*a*]pyrene; 10-OH-HCPBP, 10 hydroxycyclopenta[*mno*]benzo[*a*]pyrene, E2, estradiol; EE2, ethinylestradiol; 2,4-DHBP, 2,4 dihydroxybenzophenone; DES, diethylstilbestrol. hSULT1E1 results were adapted from (Reinen 2006).

Figure 4. Differences between mSULT1E1 (pink) and hSULT1E1 (grey). Both structures display one salt-bridge near E2, Arg23-Asp21 and Lys85-Asp22 in murine and human SULT1E1, respectively.

Figure 5. (A) The human SULT1E1 dimer. PAP is displayed in ball and stick and E2 in space-fill. The dimer interface residues are also displayed. The regions that lose their secondary structure in the simulations of the human monomer are displayed in orange and indicated by arrows. (B) Close-up of the dimer interface and the hydrogen bonds between the monomers. The outermost hydrogen bond between Lys264 and Glu273 is disrupted in the crystallized dimer, due to the mutation V269E, displayed in pink.

Figure 6. Distance between the centres of geometry of α-carbons of the backbone of residues 263-273 in each hSULT1E1 monomer. E2=17β-estradiol; E1=estrone; DES=diethylstilbestrol; DIS=dienestrol; OHP=1-hydroxypyrene. For each substrate the values are averages over 10 1 ns simulations.

Figure 7. RMS fluctuation of the atoms of E2 simulated in complex with human SULT1E1, dimer and monomer, and murine SULT1E1. Values are averages of 10 simulations. The

average RMS fluctuations over all atoms are 1.03, 1.13, 1.22 and 0.98 Å for hSULT1E1 A, B, hSULT1E1 monomer and mSULT1E1, respectively.

Figure 8. The last snapshots of 10 1 ns simulations of E2 in human (A) and murine (B) SULT1E1. The protein structures (in grey) are the starting structures of the simulation. The starting position of E2 is depicted in dark pink. Substrate structures that are in the catalytic position are displayed in cyan. Structures that have left the catalytic position are depicted in light pink.

Table 1. Structures of 14 EDCs selected for IC50 measurements.

Compound name	*Structure*
Estriol (E3)	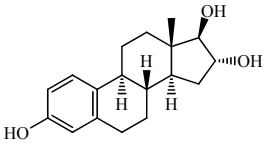
17α-Ethinylestradiol (EE2)	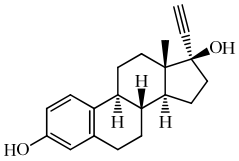
17α-Estradiol (αE2)	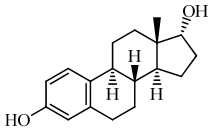
17β-Estradiol (E2)	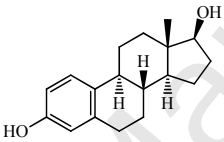
Estrone (E1)	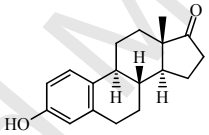
Diethylstilbestrol (DES)	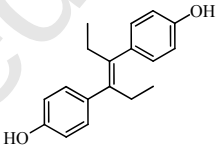
Hexestrol	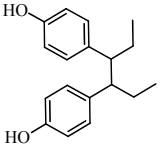
Genistein	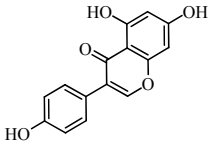
Zearalenone	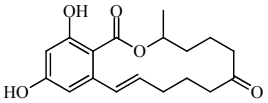
Progesterone	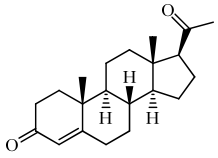

Testosterone	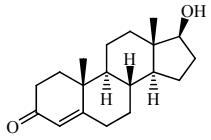
Resveratrol	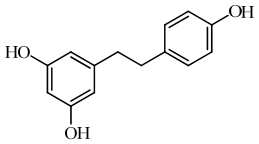
Dienestrol (DIS)	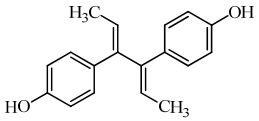
Enterolactone	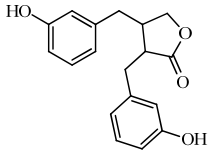

Table 2. IC_{50} and K_i values of a set of 14 inhibitors of mSULT1E1- and hSULT1E1-mediated 1-hydroxypyrene sulfo-conjugation by EDCs.

Compound	IC_{50} (nM)[a]		K_i (nM)[b]	K_i (nM)[b]	Ratio[c]
	mSULT1E1	hSULT1E1	mSULT1E1	hSULT1E1	
Estriol	41.9 ± 3.60	36.2 ± 4.10	23.0 ± 3.06	9.21 ± 1.55	2.50 ± 0.537
17α-Ethynylestradiol	50.4 ± 6.70	60.7 ± 5.80	27.7 ± 4.63	15.4 ± 2.43	1.79 ± 0.412
β-Estradiol	50.6 ± 14.9	27.7 ± 2.50	27.8 ± 8.66	7.05 ± 1.09	3.94 ± 1.37
α-Estradiol	55.4 ± 7.20	59.1 ± 6.10	30.5 ± 5.02	15.0 ± 2.44	2.02 ± 0.468
Estrone	73.2 ± 12.2	5.45 ± 0.49	40.2 ± 7.85	1.39 ± 0.21	29.0 ± 7.21
DES	670 ± 78.0	746 ± 83.0	368 ± 56.9	190 ± 31.8	1.94 ± 0.442
Hexestrol	2140 ± 270	543 ± 87.0	1176 ± 191	138 ± 28.1	8.51 ± 2.21
Genistein	3150 ± 810	1300 ± 120	1731 ± 479	331 ± 51.4	5.23 ± 1.66
Zearalenone	3840 ± 770	642 ± 79.0	2110 ± 474	163 ± 28.7	12.9 ± 3.68
Progesterone	6560 ± 1350	2780 ± 390	3605 ± 827	707 ± 133	5.10 ± 1.51
Testosterone	6990 ± 2550	28100 ± 4300	3841 ± 1455	7150 ± 1410	0.537 ± 0.229
Resveratrol	11600 ± 2600	1860 ± 400	6375 ± 1569	473 ± 118	13.5 ± 4.71
Dienestrol	20300 ± 4200	2140 ± 250	11156 ± 2572	545 ± 93.2	20.5 ± 5.88
Enterolactone	29700 ± 5200	1250 ± 230	16322 ± 3304	318 ± 70.8	51.3 ± 15.4

[a] Values are means ± SD ($n \geq 3$).

[b] Calculated as $K_i = IC_{50} / (1 + S/K_m)$, S = substrate concentration. S(mSULT1E1) = 250 nM , S(hSULT1E1) = 18.75 nM. K_m(mSULT1E1) = 305 nM, K_m(hSULT1E1) = 6.4 nM.

[c] Ratio is defined as K_i (mSULT1E1)/K_i (hSULT1E1)

Table 3. Percentage of time that the 3-hydroxyl of E2 is within 3.5 Å of the Nε of the catalytic histidine, His107, and the RMS deviation of the substrate atoms during simulations of the human dimer and the human crystal.

	Human SULT1E1 dimer		Human SULT1E1 crystal	
	Monomer A[1]	monomer B[1]	monomer A[2]	monomer B[2]
% time 3β-OH < 3.5 Å from His107Nε	38.1	58.7	10.8	60.8
RMS deviation substrate (Å)	2.1	1.8	1.2	1.2

[1] Average over 10 simulations

[2] Average over two identical monomers in the crystal

Table 4. Average occurrence of a hydrogen bond between the 3-hydroxyl of E2 and His107Nε, and the RMS deviation of the substrate atoms during simulations of the SULT1E1 human dimer and the free human monomer A.

	Human SULT1E1 dimer		Human SULT1E1 monomer A
	monomer A[1]	monomer B[1]	monomer A[1]
Hbond occurrence (%)	28.6	32.1	29.1
RMS deviation substrate (Å)	2.1	1.8	2.5

[1] Average over 10 simulations

Table 5. Ligand-protein hydrogen bonds and active site structure for various SULT1E1 complexes

Compound	Hbond His107/108 Nε [a] (%)	N_{50} [b] (%)	Hbond Lys85Nζ/ ASN86Nδ [c] (%)	Hbond ligand Asp22Oδ/ Arg23Nε/η [d] (%)	Distance Lys85Nζ - - His107Nε/ Asn86Cγ - His108Nε [e] (Å)	Distance Asp22Cγ - His107Nε/ Arg23Cζ - His108Nε [f] (Å)	O-O distance ligand [g] (Å)	N_{2HB} [h] (%)	RMS ligand [i] (Å)
E2									
hSULT1E1A	28.6	20	11.3	21.4	16.4	15.9	10.9	0	2.09
hSULT1E1B	32.1	40	9.39	13.6	16.4	16.2	10.9	10	1.84
mSULT1E1	51.6	50	41.1	8.78	13.7	14.6	10.9	50	1.88
E1									
hSULT1E1A	6.24	0	5.55	-	16.1	15.6	10.7	0	1.36
hSULT1E1B	17.9	20	5.32	-	16.4	15.8	10.7	0	1.73
mSULT1E1	30.1	30	16.1	0.59	13.4	14.9	10.7	0	1.79
DES									
hSULT1E1A	5.54	0	14.6	83.4	16.4	15.2	11.9	10	2.84
hSULT1E1B	6.75	0	21.3	49.4	16.3	15.8	11.9	10	3.00
mSULT1E1	53.4	50	21.9	13.4	13.5	14.8	12.0	40	2.28
DIS									
hSULT1E1A	9.13	10	4.12	0	16.3	16.1	11.9	0	3.23
hSULT1E1B	6.42	0	33.2	86.7	16.1	15.3	12.0	30	3.03
mSULT1E1	49.7	50	20.7	13.9	13.7	15.0	12.0	50	2.30
OHP									
hSULT1E1A	32.3	30	-	-	-	-	-	-	3.04
hSULT1E1B	42.0	40	-	-	-	-	-	-	3.00
mSULT1E1	32.0	20	-	-	-	-	-	-	2.86

[a] Average occurrence of a hydrogen bond between the ligands and His107Nε (human) or His108Nε (mouse).

[b] Percentage of independent simulations in which the hydrogen bond to His107Nε (human) or His108Nε (mouse) occurs for more than 50% of the simulation time.

[c] Average occurrence of a hydrogen bond between the ligands and Lys84Nζ (human) or Asn86Nδ (mouse).

[d] Average occurrence of a hydrogen bond between the ligands and Asp22Oδ (human) or Arg23Nε/η (mouse).

[e] Average distance between Lys84Nζ and His107Nε (human) or Asn86Nδ and His108Nε (mouse).

[f] Average distance between Asp22Cγ and His107Nε (human) or Arg23Cζ and His108Nε (mouse).

[g] Average distance between the two hydroxyl O-atoms in the ligands.

[h] Percentage of independent simulations in which both hydroxyl groups of the ligands are simultaneously engaged in hydrogen bonds with the protein.

[i] Average RMS deviation of the ligand over the simulations. The average is taken over 10 simulations for each ligand.

Figure 1A

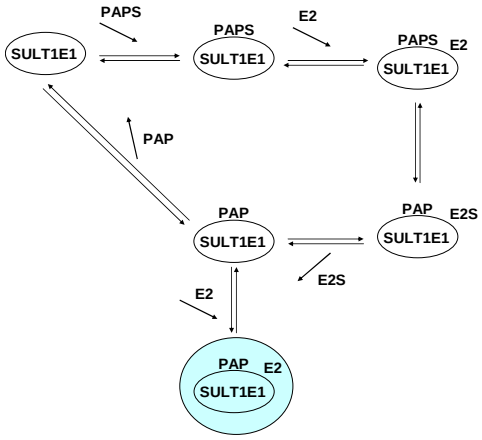

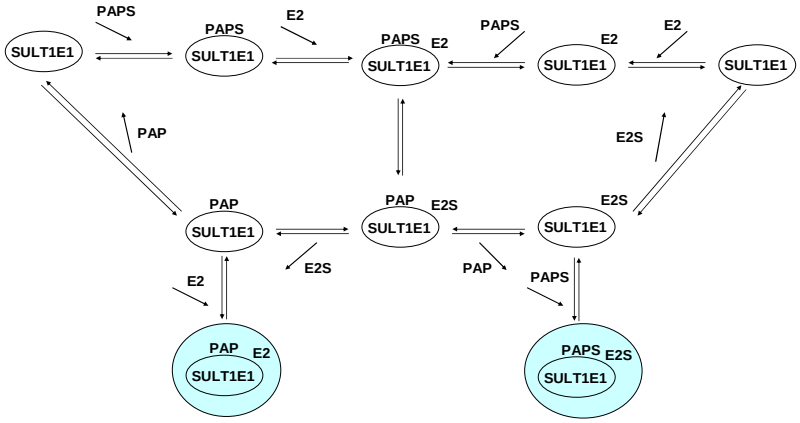
PAPS
SULT1E1
PAPS
SULT1E1
E2
PAPS
E2
SULT1E1
PAPS
SULT1E1
E2
E2
SULT1E1
PAP
E2S
PAP
SULT1E1
PAP
E2S
SULT1E1
E2S
SULT1E1
E2
E2S
PAP
PAPS
PAP
E2
SULT1E1
PAPS
E2S
SULT1E1

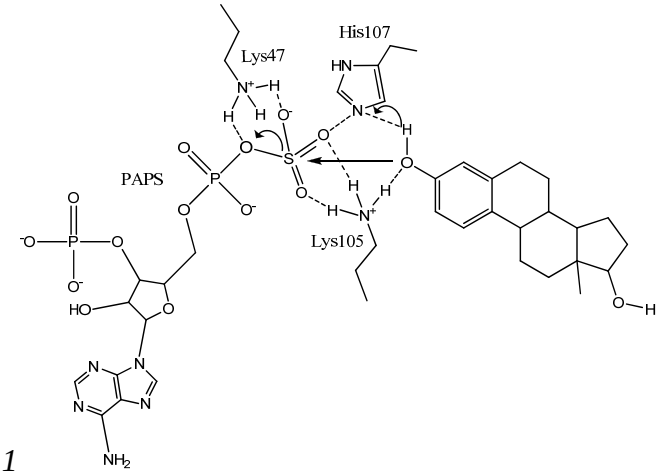

Step 1

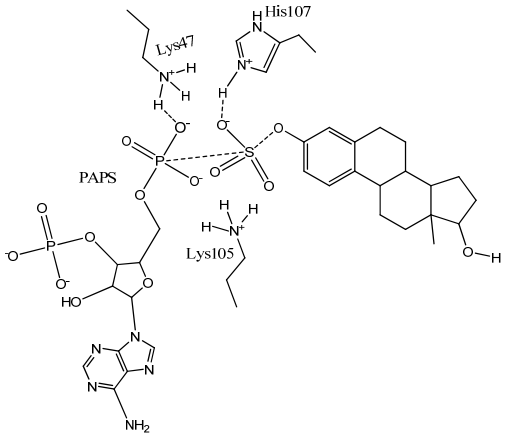

Step 2

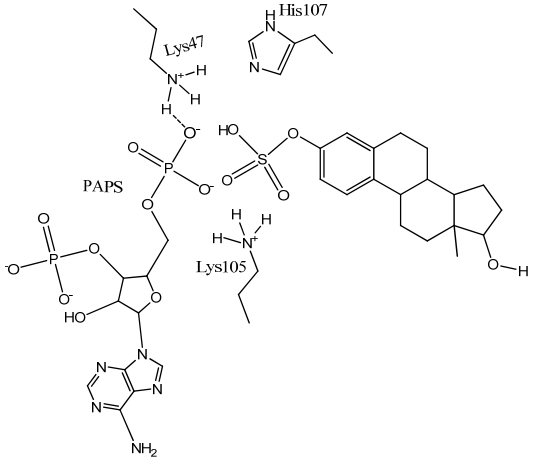

Step 3

Figure 3

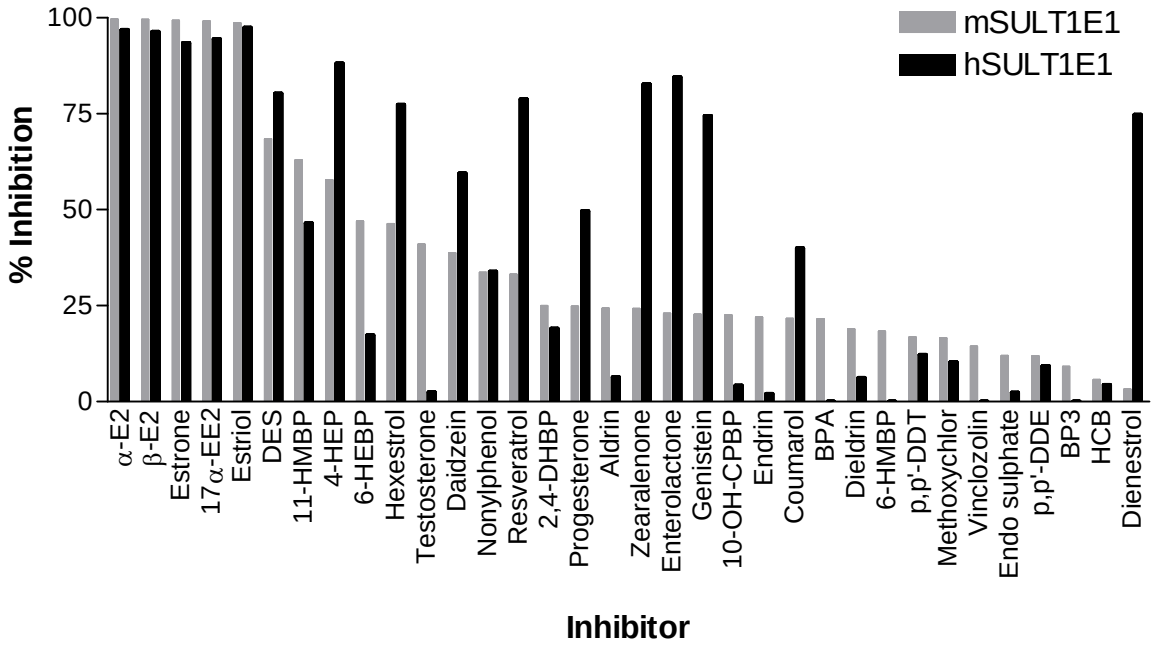

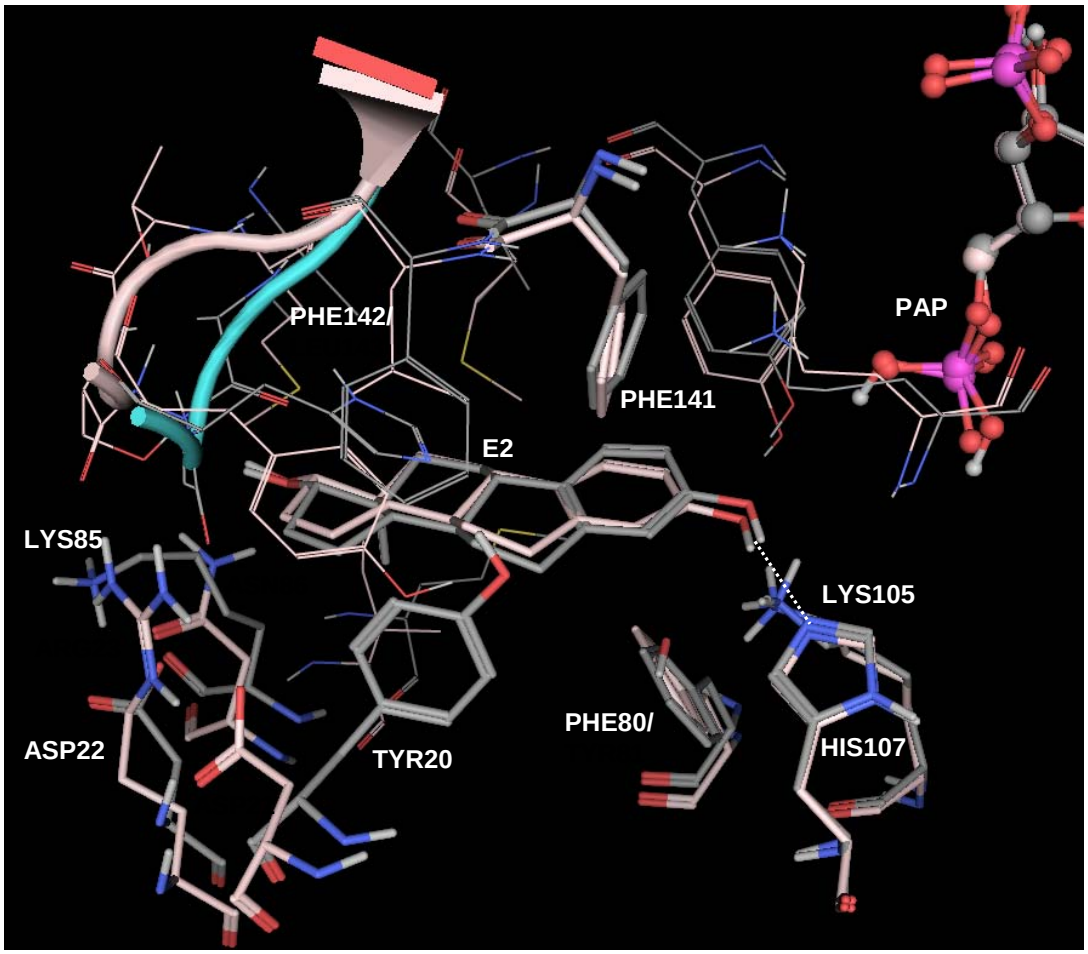
PHE142/
PAP
PHE141
E2
LYS85
LYS105
PHE80/
ASP22
TYR20
HIS107

Figure 5A

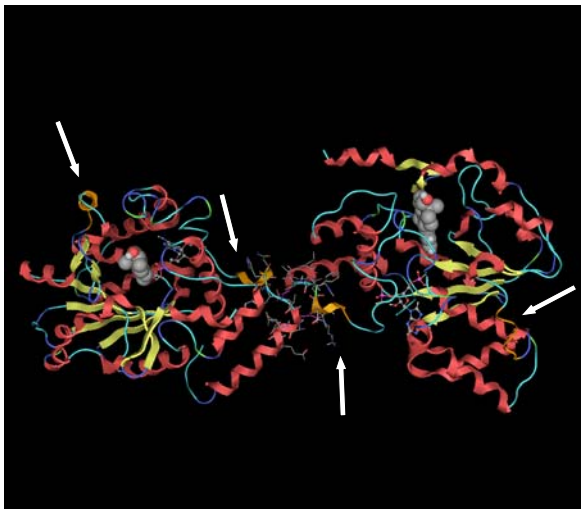

Figure 5B

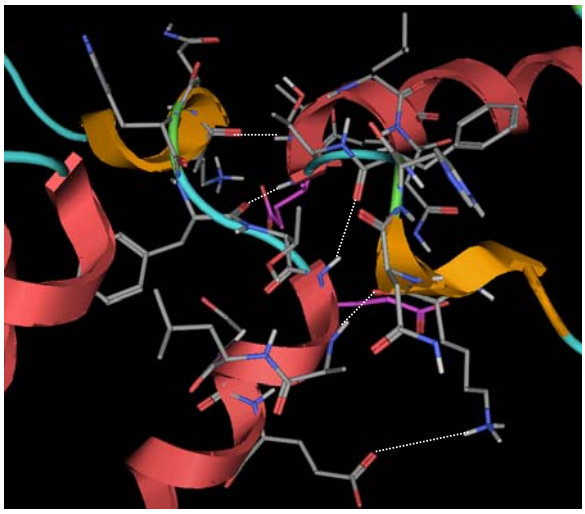

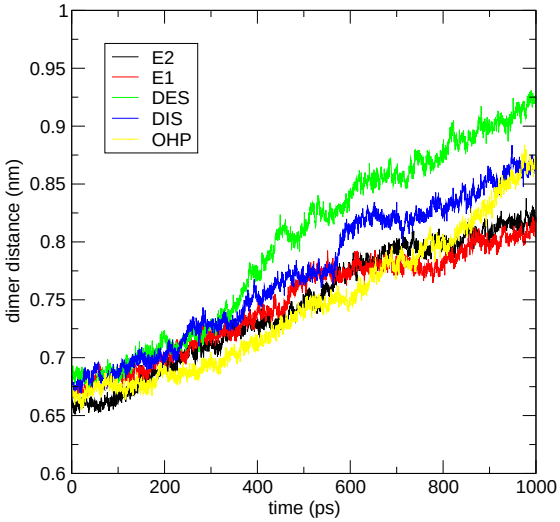
E2
E1
DES
DIS
OHP
dimer distance (nm)
time (ps)
1
0.95
0.9
0.85
0.8
0.75
0.7
0.65
0.6
0
200
400
600
800
1000

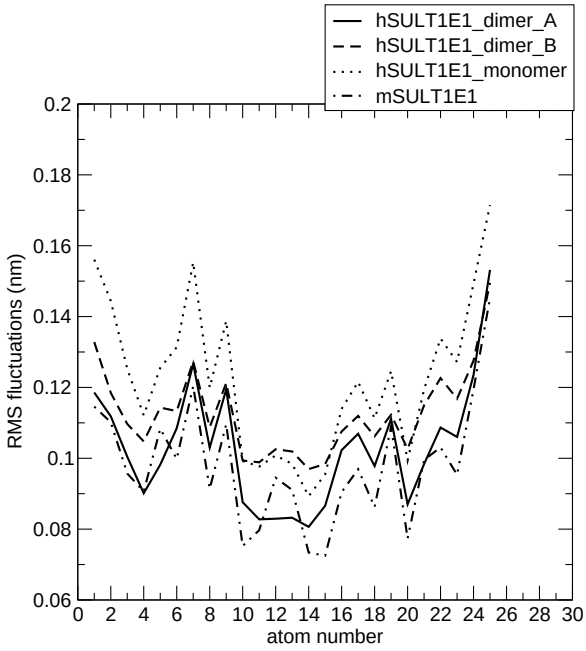
hSULT1E1_dimer_A
hSULT1E1_dimer_B
hSULT1E1_monomer
mSULT1E1
RMS fluctuations (nm)
atom number
0.2
0.18
0.16
0.14
0.12
0.1
0.08
0.06
0 2 4 6 8 10 12 14 16 18 20 22 24 26 28 30

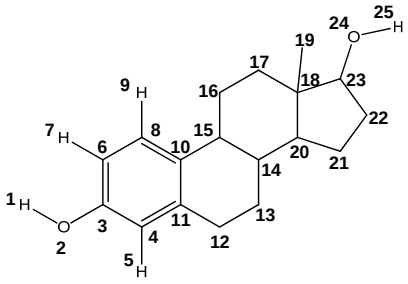
1 H
2
3
4
5 H
6
7 H
8
9 H
10
11
12
13
14
15
16
17
18
19
20
21
22
23
24
25 H

Figure 8A

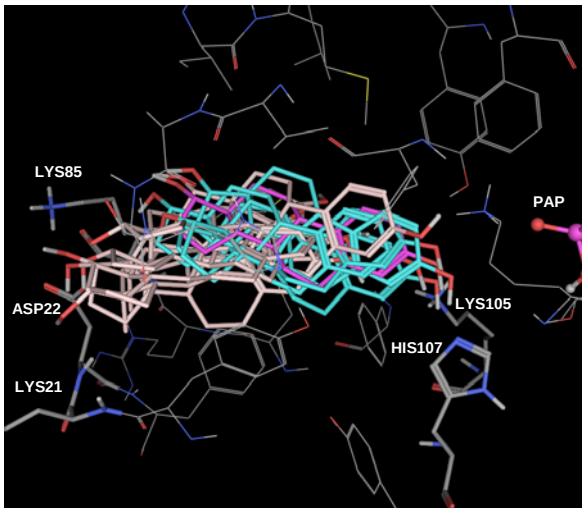

Figure 8B